Investigating how the formation process of Cu nanoparticles can affect their CO_2RR activity

Elena Gazzarrini and Francesca Baletto
Physics Department, King's College London, WC2R 2LS, London, UK
(Dated: April 3, 2020)

We propose a multiscale numerical model to estimate how the formation process to produce Cu nanoparticles affect their catalytic activity for CO_2 reduction. Although this reaction can lead to multiple hydrocarbon products, we focus our attention on the hydrogenation to methane for which the protonation of CO to CHO is the rate-limiting step. Using classical molecular dynamics, we model three formation processes, namely the annealing from a liquid droplet; the solid growth proceeding via the addition of single atoms; and the coalescence of two nanoparticles. We explore the size range between 1.5-2.5 nm. Our model analyses the evolution of the generalised coordination number during the formation process and employs an available structure-energy relationship to estimate the specific and the mass activities. We show that each formation process leads to a different size-behaviour for the activity. The obtained mass activities range between 5.2-11.2 mA/mg. There is a clear evidence that surface roughness and defects improve catalytic performance of Cu nanoparticles for the CO protonation. Quite surprisingly, the activity has a different size-trend depending on the formation process. While the annealing has a monotonic decrease with the nanoparticle size, larger and more defected nanoparticles obtained via the one-by-one growth - although depending on the shape of the initial seed - are the most active. Coalescence has a non-monotonic behaviour with size strongly depending on how fast necks and interfaces of the individual nanoparticles rearrange.

I. INTRODUCTION

Electroreduction of CO_2 represents a promising approach toward artificial carbon recycling for addressing global challenges in energy and sustainability. As CO_2 is thermodynamically stable and kinetically inert[1,2], its efficient conversion requires the use of catalysts capable of selectively reducing CO_2 to valuable (oxygenated) hydrocarbon products at low overpotential. In recent years, CO_2 conversion using electrochemical catalysis approaches has attracted great attention for its several advantages: (1) the process is controllable by electrode potentials and reaction temperature; (2) the supporting electrolytes can be fully recycled so that the overall chemical consumption can be minimized to water only; (3) the electricity used to drive the process can be obtained by employing renewable energies; and (4) the electrochemical reaction systems are compact, modular, on-demand, and easy for scale-up applications[3–6]. Metallic nanoparticles (NPs) are deemed to be likely candidates for the purpose of heterogeneous catalysis in electrochemical fuel cells[7–9]. To propose robust design-rules for nanocatalysts (their size, shape, chemical composition and ordering) avoiding a costly and ineffective trial-and-error procedure, two factors should be simultaneously taken into account: (i) the variety of adsorption sites per each isomer[10], which influences both activity and selectivity, and (ii) the coexistence of different geometries, eventually related to their formation process[11]. Out of the polycrystalline metals, copper (Cu) is the only heterogeneous catalyst that has shown a propensity to produce valuable hydrocarbons, aldehydes and alcohols from electrochemical CO_2 Reduction Reaction (CO_2RR)[1]. Even if copper has already largely been used as a catalyst to reduce the CO_2[1,2,5,6,12–20,22–24,26,27,29,51], it is still a challenge to reach higher efficiencies[39]. Here for the first time, we adopt our recently proposed nanoCHE model[45,68] to the protonation of CO into CHO. The catalytic performance of Cu is closely associated with the electronic structure of the active site[40,42]. The prediction of the catalytic activity of Cu by means of the atop generalised coordination number, a suitable geometrical descriptor to classify every adsorption sites, provides a robust structure-energy relationship, to be combined with the nanoCHE model[22,43,47]. Furthermore we demonstrate that the formation process can significantly affect the Cu activity. We model freezing, growth atom-by-atom and coalescence. The mass activity of structures resulting from freezing decreases with the increase in size. Growth from the subsequent addition of atoms improves NP activity while coalescence does not show any particular size-behaviour. We anticipate that our results may be of interest to the experimental communities - who could use our findings to engineer tailored experiments.

II. METHODOLOGY

The reaction pathways from CO_2 to CH_4 on Cu have been established by Peterson et al.[20,21] as :

$$\begin{aligned} &CO_2 \xrightarrow{H^*} COOH^* \xrightarrow{H^*} CO^* \xrightarrow{H^*} CHO^* \xrightarrow{H^*} CH_2O^* \\ &\xrightarrow{H^*} OCH_3^* \xrightarrow{H^*} O^* + CH_4 \xrightarrow{H^*} OH^* \xrightarrow{H^*} H_2O \quad , \end{aligned} \tag{1}$$

where * stands for adsorbed molecules. For CH_4, the rate limiting step is considered to be the the protonation of adsorbed CO to make adsorbed CHO[23]. The binding energy difference between the two adsorbates will dictate the relative activity of each NP facet. The activity of a NP is the rate of a specific reaction happening on its surface; it ca be normalised to the real NP's area (leading to the specific activity, SA), or to the NP's mass (leading to the mass activity, MA). The SA determines how much current is achieved at a certain applied overpotential[12].

For the case of the electrochemical reduction of carbon dioxide to CH_4, which involves the atop adsorption of CO, the atop Generalized Coordination Number, aGCN, , as demonstrated by Zhao et al.[22]. The core assumption of this model is that the reaction free energy ΔG of the rate limiting step of the reaction can be written as a function of the generalized coordination number.

To monitor the evolution of the mass activity for various nanoparticle shapes, we employ the NanoCHE model. This is an extension of the CHE model pioneered by Norskov and co-workers[71]. It allows to translate changes in the coordination of active sites - because of the intrinsic structural

fluxionality of nanoparticles[59–61]- into potential changes of their activity. This approach also enables to simulate a linear sweep voltammetry experiment upon metallic nanosystems with a wide variety of non equivalent adsorption sites.

The atop generalised coordination number (aGCN) - which has been proven to be a robust activity descriptor[47] - is introduced and its relation to the reaction free energy ΔG for CHO formation is taken from Zhao et al.[22], and reported in the turquoise box in Figure 1. At a certain time t of the evolution, at a temperature T, and at an applied voltage U, the current density is[70]

$$j_{NP}(t,T,U) = \sum_{i\in\{\text{aGCN}\}} C\ \frac{\Omega(i)}{N_{sites}}\ \ i\ \ e^{\beta(\Delta G(i)-neU)} \quad , \quad (2)$$

where $aGCN_i$ equals $\sum_j \frac{CN_j}{CN_{max}}$. CN_j is the nominal coordination number of the j-neighbouring atoms of i calculated within a cut-off distance r_{cut}, defined as the first minimum in the pair-distance distribution function (PDDF) and CN_{max} is set to 12. T is kept at 300 K, since catalysis occurs usually at room temperature. The temperature used in the CMD simulations should be considered as a tool to accelerate rate events. N_{sites} corresponds to the number of surface sites. The pre-factor C is fitted to reproduce the specific activity of low-Miller index surfaces[70] and by combining the experimental value of the IV-curve of a 24 nm cube.[46] We fix C to -3.01 $\cdot$ 10^{14} mA/cm^2.

The mass activity (MA) at a certain applied potential U^*, here 1.1 V, is

$$\text{MA} = \frac{j^*_{\text{NP}} \cdot \text{A}_{\text{surf}}}{\text{M}} \quad , \quad (3)$$

where the mass is the number of atoms N in the NP multiplied by their atomic mass, i.e. 63.546 a.u. for Cu. The surface area A_{surf} is quantifiable as a function of the aGCN too, $\text{A}_{\text{surf}} = \sum_i^N 4\pi r^2_{\text{atomic}} \left(1 - \frac{\text{aGCN}(i)}{12}\right)$, where the sum is over all atoms i in the nanoparticle, and r_{atomic} is the atomic radius of the particle, namely 0.128 nm for Cu.

We model different formation processes, namely freezing, growth, coalescence, through classical molecular dynamics (CMD) simulations as available in the LoDiS package[57] and we use a common neighbour analysis (CNA)[49,50] to classify Cu-NPs into geometrical families, namely FCC, Icosahedra (Ih) and Decahedra (Dh), as well as defects formation, i.e. re-entrances and elongated concavities, and the formation of twin planes, grain boundaries, and five-fold axes. A velocity-Verlet algorithm[56] is exploited to evolve Newton's Equation of motion with a time step of 5 fs and the atomic interaction is described by the Rosato-Guillope-Legrand (RGL) potential[57], with parameters for Cu from[57]. An Andersen thermostat is used to control the temperature. Per each system we accumulate four independent simulations and average them. The NPs vary from a size of 110 to 976 atoms, i.e. 1.5-2.5 nm. The geometries used are FCC polyhedra, namely Octahedra (Oh) and their regular truncation (To), Marks-Decahedra (MDh), Icosahedra (Ih) and defected Icosahedra (dIh) resulting from a basin-hopping algorithm at not-magic sizes[62].

The annealing of a liquid droplet at 147, 250, 561, 585, 586, 891, and 976 atoms follows the iterative Molecular Dynamics (itMD) algorithm[57]. This is various and concatenated canonical NVT runs, where the temperature is lowered from 1200 K to 400 K at a rate of 5 K/ns. We model the atom-by-atom growth as described in detailed in[62], starting from three seed of similar size as Cu_{146} (Oh), Cu_{147} (Ih) and Cu_{201} (To) up to 996 atoms, where atoms are deposited every 4 ns at 600 K. Coalescence is the process by which two clusters are made colliding along the z axis. Each nanoparticle is free to move at 600 K, and we analyse the first 0.05 ns of their dynamics.

The workflow of the proposed multiscale numerical strategy is visually represented in Figure 1.

III. RESULTS AND DISCUSSION

Surface atoms are believed to correspond to a coordination between 2 and 9 are considered: only such atoms are considered, in order to be consistent with Zhao et al.[22]. The aGCN distribution is more widely spread for liquid structures, since they are disordered and low-coordinated; it narrows down to specific signatures when the temperature is decreased. NPs resulting from growth are highly undercoordinated, and are thus expected to produce a higher current density. The Ih evolution produces more undercoordinated sites than the Oh or the To evolution. Coalescence leads to defected or amorphous elongated structures. The aGCN distributions at different sizes produced by the three processes can be seen in Figure 2.

Small NPs (1.5 nm) produced by growth are low-coordinated, presenting aGCN values of around 2. This will increase their current density. Frozen droplets of sizes between 490 and 850 atoms are more highly coordinated than collided and grown ones at the same sizes. Coalescence of a system composed of 581 atoms leads to a NP which is less coordinated than one resulting from growth.

Some NP snapshots of structures at various sizes are displayed in Figure 3.16 to perform useful comparisons.

Cu_{147} is expected to be highly active, being its surface extraordinarily low-coordinated. It is surprising how the simulation time is sufficient to bring it to a perfectly ordered Ih. Frozen NPs become defected Ih, Dh and FCC structures, preserving their initial spherical shape. On the contrary, the growth of both Oh and To presents structures with many (111), (100) and (211) facets. The Oh exhibits triangular facets, while the To hexagonal ones. The Ih evolution proceeds with a layer-by-layer deposition, maintaining its Ih resemblance. Collided NPs' final geometries are elongated and, in most cases, amorphous. The neck formation leads to a peak in highly-coordinated sites.

The NP coordination is employed to obtain IV curves for the protonation of CO to CHO. The current density results range from -0.12 mA/cm^2 (frozen Cu_{561}) to -0.69 mA/cm^2 (liquid Cu_{147}) at an applied potential of -1.11 V, and they are displayed in Figure 4.

It can be seen how in the coalescence process the size does not influence the current density evolution. The collision of a mDh with Ih and dIh (sizes of 581 and 719 atoms) lead to NPs carrying more current density than other collided structures. Such high js are only achieved at liquid small NPs. The case of liquid small NPs is extraordinary; liquid Cu_{147}, due to its small size and high number of low-coordinated sites carries an extremely high current density. Some quantum effects are not to be excluded in this case. Frozen NPs carry a low current density; the only ones that can be compared to other results are Cu_{250} and Cu_{586}, which are disordered enough to exhibit low-coordinated sites: the first produces a current density equivalent to an FCC grown to 250 atoms, while the latter

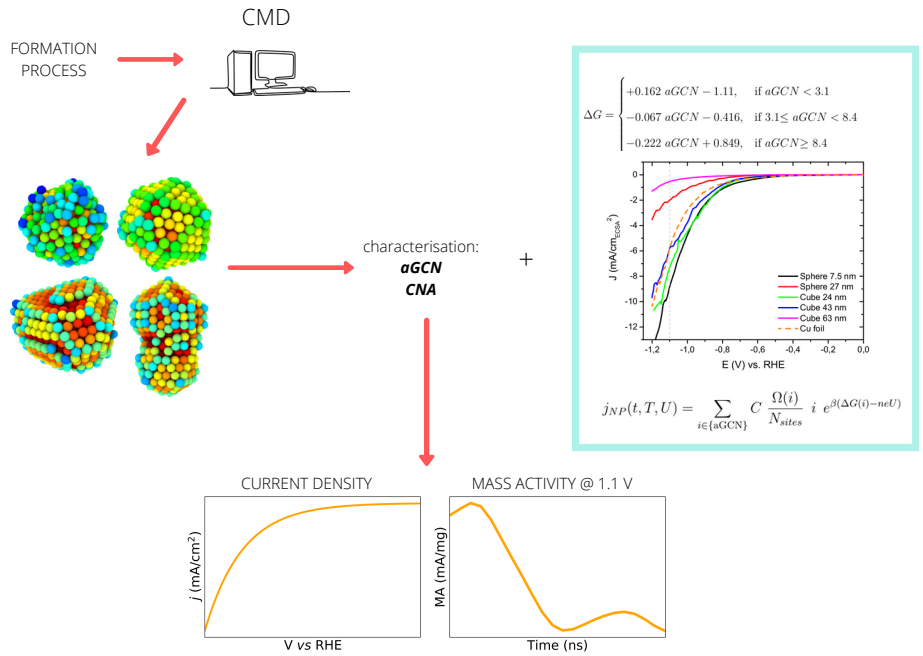

FIG. 1: Workflow. The formation process (freezing, growth, coalescence) is investigated by means of classical molecular dynamics (CMD). Various shapes and sizes are produced. They are geometrically characterized through a CNA and by analysing their aGCN distribution. By combining our data with other studies[22,46] (reported in the box) the current density j produced by the NP is calculated, to then measure the cluster's mass activity and quantify their catalytic properties.

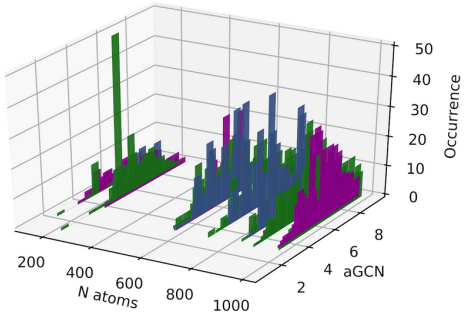

FIG. 2: aGCN occurrence at 600K for different processes and different cluster dimensions. represents freezing, growth and coalescence.

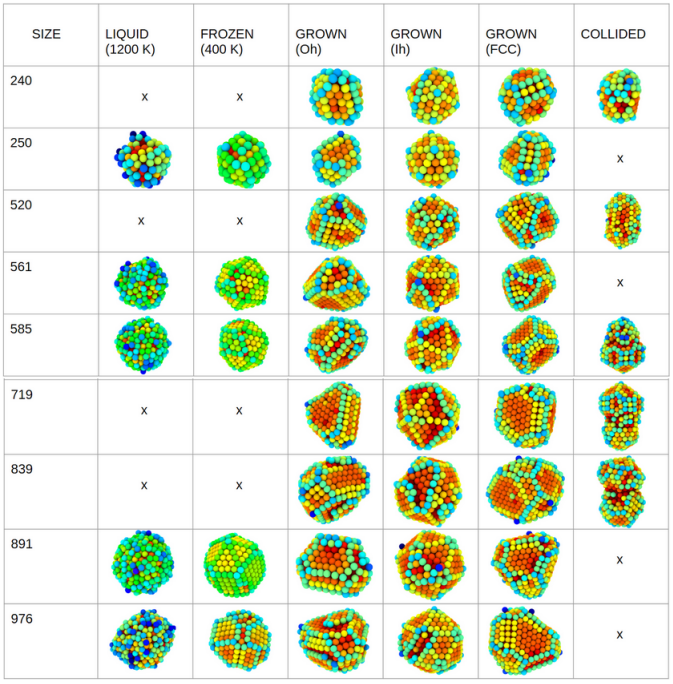

FIG. 3: Pictorial representation of common snapshots found listed per each formation processes for Cu-nanoparticles. Atoms are coloured accordingly to their atop GCN (red 2 and blue 9) following the color gradient .

to an Oh grown to 976 atoms. Liquid structures are better than frozen ones at equivalent sizes, apart the case of Cu_{250}, since it is the only one starting from a non-magical size. Within the grown structures, the Ih evolution leads to less current density at every size considered. At very small (250 atoms) and very big (976 atoms) sizes the FCC evolution produces more current density, while at intermediate sizes the Oh seems to be more favourable for the CO_2 activity.

To obtain the mass activity of the cluster, surface area calculations are performed. The surface area noticeably decreases throughout the freezing process, dropping from values of 1.2-5.4 $\cdot 10^{-15}$ cm^2 (the highest achieved) to 1-3.8 $\cdot 10^{-15}$ cm^2. The surface area of grown structures increases monotonically with size, leading to values between 1-3.5 $\cdot 10^{-15}$ cm^2. Coalescence leads to structures with a surface area of 1.4-3.6 $\cdot 10^{-15}$cm^2.

The MAs calculated through Equation 3 are reported in Figure 5.

The liquid droplet of Cu_{147} is extremely active, as expected from its high current density. The results proves that mall NPs with low-coordinated surface atoms are more favorable for CO_2 dissociation than larger particles[24]. Liquid NPs are more active than solid ones due their lower-coordination: the only exception is, again, given by the freezing of a non-magical size, Cu_{250}. The low current density produced by large NPs and their larger mass result in a restricted mass activity of large structures produced by freezing, compared to smaller ones resulting from the same formation process. Small grown NPs made of around 250 atoms report a MA between 6.5 mA/mg and 7.5 mA/mg, noticeably lower than the activity of a frozen NP at the same size, which is about 4.6 mA/mg. There are, however,

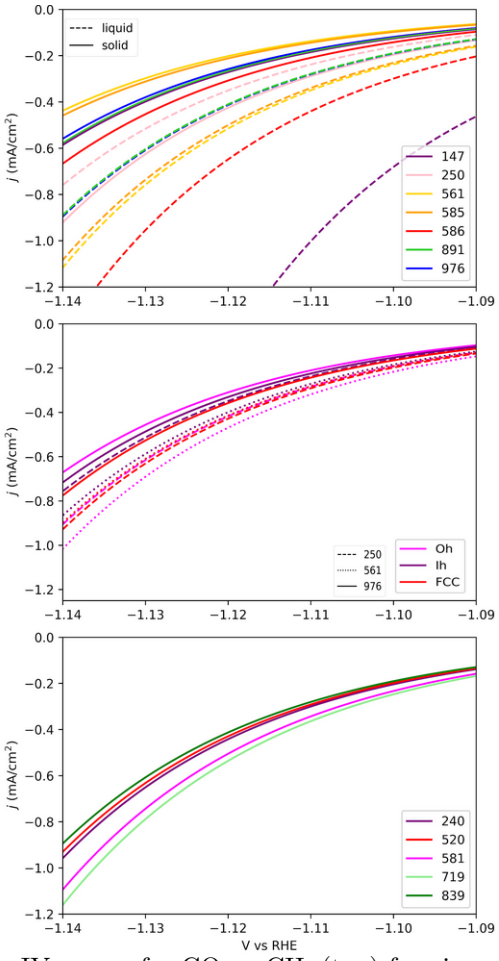

FIG. 4: IV curves for CO → CH. (top) freezing process, dashed line refers to the melted phase and solid-line for the frozen object; (middle) growth one-by-one, different colours refers to different initial seed; (bottom) coalescence after 0.05 ns.

a few exceptions to the monotonically increasing mass activity with the decrease of NP's size in freezing processes, due to the free energy dependence on structure's coordination (Cu_{585} is less active than Cu_{561}, for instance). The increase in surface area with the increase in size for one-by-one growth processes leads to a monotonically increasing relationship between activity and NP's size. From sizes of 550 to 650 atoms the Oh evolution seems the most promising one, with a MA of around 8.5 mA/mg, high compared to the value of 7.5 mA/mg produced by frozen Cu_{561}. At this stage (2 nm) already, grown NPs appear to be more active than frozen ones.

The collisions between a mDh (Cu_{434}) and an Ih (Cu_{147}) produces 10.3 mA/mg, being more active than the collision of a mDh with a dIh or a To. Collided Ih appear to be better catalysts than other collided shapes.

IV. CONCLUSIONS

The Cu catalytic activity for protonation of CO to CHO for CO_2RR to CH_4 is successfully investigated through the NanoCHE model, and is found to follow a different size-trend depending on the CMD formation process. Small liquid droplets reach the highest results achieved, with a mass activity equivalent to 29.4 mA/mg. Freezing processes are characterised by a monotonically increase in mass activity with the decrease of NP's size, while the opposite behaviour

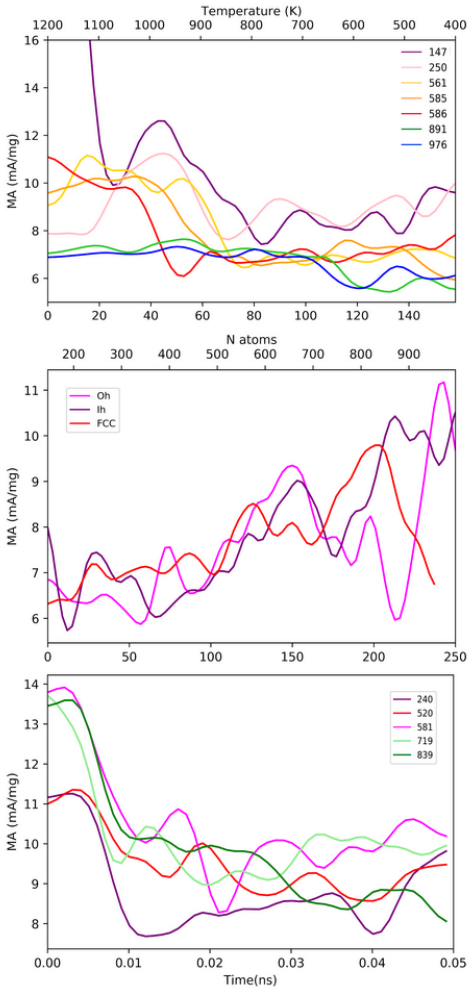

FIG. 5: Mass activity evolution in mA/mg. The lines have been smoothed using a Gaussian fit to make them more readable. The plots refer to (top) freezing process, (middle) growth one-by-one and (bottom) coalescence. The legends for freezing and coalescence represent the number of Cu atoms.

is observed in one-by-one growth processes, where larger and more defected NPs are the most active. At sizes of 1.6 nm the mass activity is equivalent to 9.6 mA/mg and 7 mA/mg for frozen droplets and deposited NPs respectively, while at larger sizes of 2.5 nm grown structures produce 11.2 mA/mg, and frozen ones 5.2 mA/mg. NPs produced by collision report an activity which is dependent on how fast necks and interfaces of the individual nanoparticles rearrange, rather than on their sizes.

V. ACKNOWLEDGEMENTS

The authors would like to thank Matteo Tiberi, Robert Jones, Laia Delgado and Armand Auqier for their insightful suggestions. FB thanks the "Towards an Understanding of Catalysis on Nanoalloys" (TOU- CAN) EPSRC Critical Mass Grant (EP/J010812/1) as does KR (ER/M506357/1). All the authors are grateful to the Royal Society, RG 120207 and the IT support offered by the NMS Faculty.

[1] C. Hahn et al. *Engineering Cu surfaces for the electrocatalytic conversionof CO_2: Controlling selectivity toward oxygenates and hydrocarbons.* PNAS, 2017, 6, 114 (23) 5918-5923.

[2] X. Kang et al. *Highly efficient electrochemical reduction of CO_2 to CH_4 in an ionic liquid using a metal–organic framework cathode.* Chem. Sci.,2016,7,266.

[3] A. S. Agarwal et al. *The electrochemical reduction of carbon dioxide to formate/formic acid: engineering and economic feasibility.* ChemSusChem, 2011, 4 , 1301 —1310.

[4] Y. Hori et al. *Electrocatalytic Process of CO Selectivity in Electrochemical Reduction of CO_2 at Metal Electrodes in Aqueous Media.* Electrochim. Acta 1994, 39, 1833-1839.

[5] S. Min et al. *Low Overpotential and High Current CO_2 Reduction with Surface Reconstructed Cu Foam Electrodes.* Nano Energy 2016, 27, 121–129.

[6] D. Raciti et al. *Highly Dense Cu Nanowires for Low-Overpotential CO_2 Reduction.* Nano Lett. 2015, 15, 10, 6829-6835.

[7] C. Anmin et al. *Stabilizing metal nanoparticles for heterogeneous catalysis.* Phys.Chem.Chem.Phys., 2010, 11,12(41):13499-510.

[8] R. Schlögl. *Heterogeneous Catalysis* Angew. Chem., Int. Ed., 2015, 54,3465–3520.

[9] I. Lee et al. *Tuning selectivity in catalysis by controlling particle shape.* Nat. Mater., 2009, 8, 132–138.

[10] J. B. A. Davis et al. *The Effect of Dispersion Correction on the Adsorption of CO on Metallic Nanoparticles.* J. Phys. Chem. A,2015, 119, 9703–9709.84.

[11] M. Foster et al. *Experimental determination of the energy difference between competing isomers of deposited, size-selected goldnanoclusters.* Nat. Commun., 2018, 9, 1323.

[12] S. Nitopi et al. *Progressand Perspectives of Electrochemical CO_2 Reduction on Copper in Aqueous Electrolyte.* Chem. Rev. 2019, 119, 7610-7672.

[13] K. Manthiram et al. *Enhanced electrochemical methanation of carbon dioxide with a dispersible nanoscale copper catalyst.* J.Am. Chem. Soc. 136:13319–13325.

[14] FS Roberts et al. *High selectivity for ethylene from carbon dioxide reduction over copper nanocube electrocatalysts.* Angew Chem Int Ed Engl 54: 5179–5182.

[15] D. Ren et al. *Selective electrochemical reduction of carbon dioxide to ethylene and ethanol on copper oxide catalysts.* ACS Catal 5:2814–2821.

[16] KP Kuhlet al. *New insights into the electro- chemical reduction of carbon dioxide on metallic copper surfaces.* Energy Environ. Sci. 5:7050–7059.82

[17] H. Mistry et al. *Highly Selective Plasma-Activated Copper Catalysts for Carbon Dioxide Reduction to Ethylene.* Nat. Commun.2016, 7, 1-9.

[18] C. Liet al *CO_2 Reduction at Low Overpotential on Cu Electrodes Resulting from the Reduction of Thick Cu_2O Films.* J. Am. Chem. Soc. 2012, 134,7231-7234.

[19] J. W. Vickers et al. *Electrochemical Carbon Dioxide Reduction at Nanostructured Gold, Copper, and Alloy Materials.* Energy Technol. 2017, 5, 775 –795.

[20] A. A. Peterson et al. *How copper catalyzes the electroreduction of carbon dioxide into hydrocarbon fuels.* Energy Environ. Sci. 2010, 3, 13111315.

[21] A. A. Peterson et al. *Activity descriptors for CO_2 electroreduction to methane on transition-metal catalysts.* J. Phys.Chem. Lett. 2012, 3, 251258.

[22] Z. Zhao et al. *Generalized Surface Coordination Number as an Activity Descriptor for CO_2 Reduction on Cu Surfaces.* J. Phys. Chem. C 2016, 120, 28125-28130.

[23] W. J. Durand et a. *Structure effects on the energetics of the electrochemical reduction of CO_2 by copper surfaces.* Surf. Sci. 605 (2011) 1354 – 1359.

[24] X. Zhang et al. *Optimum Cu nanoparticle catalysts for CO_2 hydrogenation towards methanol.* Nano Energy 43 (2018) 200–209.

[25] Y. Hori. *Electrochemical CO_2 reduction on metal electrodes.* Modern Aspects of Electrochemistry, Springer, New York, 2008, 89–189.

[26] W. Tang et al. *The importance of surface morphology in controlling the selectivity of polycrystalline copper for CO_2 electroreduction.* Phys. Chem. Chem. Phys. 14 (2012) 76–81.

[27] KP. Kuhl et al. *New Insights intothe Electrochemical Reduction of Carbon Dioxide on Metallic Copper Surfaces.* Energy Environ. Sci.2012, 5, 7050-7059.

[28] Hori et al. *Electrochemical Reduction of CO at a Copper Electrode.* J. Phys. Chem. B, 1997, 101 , 7075 —7081.

[29] Hori et al. *Formation of Hydrocarbons in the Electrochemical Reduction of Carbon Dioxide at a Copper Electrode in Aqueous Solution.* J. Chem. Soc., Faraday Trans. 1, 1989, 85 , 2309-2326.

[30] J. Sawyer et al. *Carbon Dioxide and the "Greenhouse" Effect.* Nature,1972, 239 , 2.83.

[31] T. Volk. *CO2 rising: the world's greatest environmental challenge.* MIT Press,2008.

[32] G. A. Olah et al. *Chemical Recycling of Carbon Dioxide to Methanol and Dimethyl Ether: From Greenhouse Gas to Renew-able, Environmentally Carbon Neutral Fuels and Synthetic Hydrocarbons.* J. Org.Chem., 2009, 74 , 487 —498.

[33] D. Y. C.Leung et al. *An overview of current status of carbon dioxide capture and storage technologies* Renew. Sust. Energ. Rev., Vol. 39, 2014, 11, 426-443.

[34] S. Chubbock et al. *Comparative Analysis of Internal Combustion Engine and Fuel Cell Rnage Extender.* SAE Int.J.Alt. Power. 5(1) 2016.

[35] R. Kortlever et al. *Catalysts and reaction pathways for the electrochemical reduction of carbon dioxide.* J. Phys. Chem. Lett. 6:4073–4082.

[36] Y. Hori. *CO_2 reduction using electrochemical approach. Solar to Chemical Energy Conversion: Theory and Application.* Springer Int., Cham, Switzerland, 191–211.

[37] A. Alshammari et al. *Metal Nanoparticles as Emerging Green Catalysts.* http://dx.doi.org/10.5772/63314.

[38] KP Kuhl et al. *Electrocatalytic conversion of carbon dioxide to methane and methanol on transition metal surfaces.* J Am Chem Soc 136:14107–14113.

[39] J. Qiao et al. *A Review of Catalysts for the Electroreduction of Carbon Dioxide to Produce Low-Carbon Fuels.* Chem. Soc. Rev. 2014,43, 631-675.

[40] T. Bligaard et al. *Ligand effects in heterogeneous catalysis and electrochemistry.* Electrochim. Acta 52 (2007) 5512-5516.79.

[41] J.K. Norskov et al. *Towards the computational design of solid catalysts.* Nat. Chem. 1 (2009) 37–46.

[42] J. Kleis et al. *Finite Size Effects in Chemical Bonding: From Small Clusters to Solids.* Catal.Lett. 141 (2011) 1067–1071.

[43] K. Rossi et al. *A genomic characterization of monometallic nanoparticles.* RSC, Issue 9, 2019.

[44] I. E. L. Stephens et al. *Understanding the electrocatalysis of oxygen reduction on platinum and its alloys.* Energy Environ. Sci., 2012, 5, 6744.

[45] K. Rossi et al. *Correlating Oxygen Reduction Reaction Activity and Structural Rearrangements in MgO-Supported Platinum Nanoparticles.* Chem. Phys. Chem. 2019, 20, 1 – 9.

[46] A. Loiudice et al. *Tailoring Copper Nanocrystals towards C_2 Products in Electrochemical CO_2 Reduction.* Angew. Chem. Int. Ed.2016, 55, 5789 –5792.

[47] M. Rück et al. *Oxygen Reduction Reaction: Rapid Prediction of Mass Activity of Un-strained Nanostructured Platinum Electrocatalysts.* J. Phys. Chem. Lett. 2018, 9,15, 4463-4468.

[48] Armand Auquier's MSci Thesis KCL, 2020, 4.

[49] J.D. Honeycutt et al. *Molecular dynamics study of melting and freezing of small Lennard-Jones clusters.* J. Phys. Chem. 1987, 91, 4950 – 4963.

[50] F. Baletto et al. *Structural properties of sub-nanometer metallic clusters.* J. Phys.Condens. Matter 2019, 31, 113001.

[51] D. Alfonso et al. *First-Principles Modeling in Heterogeneous Electrocatalysis.* Catalysts, 2018,8, 424.

[52] F. Calle-Vallejo et al. *Fast Prediction of Adsorption Properties for Platinum Nanocatalysts with Generalized Coordination Numbers.* Angew. Chem. Int. Ed. 2014, 53, 8316–8319.

[53] F. Calle-Vallejoet al. *Finding optimal surface sites on heterogeneous catalysts by counting nearest neighbors.* A. S. Science2015, 350, 185– 189.

[54] F. Calle-Vallejoet al. *Why conclusions from platinum model surfaces do not necessarily lead to enhanced nanoparticle catalysts for the oxygen reduction reaction.* Chem.Sci. 2017, 8, 2283–2289.

[55] P. Strasser et al. *Electrochemical processes on solid shaped nanoparticles with defined facets.* Chem. Soc. Rev. 2018, 47, 715–735.81.

[56] D. Frenkel et al. *Understanding Molecular Simulation* Academic Press,Inc.6277, Sea Harbor Drive Orlando, FL, United States.

[57] F. Baletto. *LoW-Dimensional Systems Molecular Dynamics.* 2019;https://github.com/orgs/kcl-tscm/teams/lodis.

[58] K. Rossi et al. *Thermodynamics of Cu Pt nanoalloys.* Sci. Rep. 2018, 8, 9150.

[59] H. Zhai et al. *Fluxionality of Catalytic Clusters: When It Matters and How to Address It.* ACS Catal. 2017, 7, 19051911.

[60] X. Xing et al. *Dynamicfluxionality and enhanced CO adsorption in the presence of coadsorbed H_2O on free gold cluster cations.* IJMS 377 (2015)393–402.

[61] A. Vargas et al. *Fluxionality of gold nanoparticles investigated by Born-Oppenheimer molecular dynamics.* Phys.Rev. B, 2009, 07, 80(19), 195421.

[62] F. Baletto et al. *Structural properties of nanoclusters: Energetic, thermo-dynamic, and kinetic effects.* Review. Mod. Phys., Vol.77, 2005, 1.

[63] A. Larsen et al. *The atomic simulation environment - a Python library for working with atoms.* J. Phys. Condens.Matter 2017, 29, 273002.

[64] A. Stukowski. *Visualization and analysis of atomistic simulation data with OVITO – the Open Visualization Tool.* Modelling Simul. Mater. Sci. Eng. 18(2010), 015012.

[65] S. Trasatti et al. J. Electroanal. Chem., 1992, 327, 353–376.

[66] C. W. Li et al. *Electroreduction of carbon monoxideto liquid fuel on oxide-derived nanocrystalline copper.* Nature, 2014, 508 , 504—507.

[67] X. Feng et al. *Grain-Boundary-Dependent CO_2 Electroreduction Activity.* J. Am. Chem. Soc., 2015, 137 , 4606 —460.

[68] K. Rossi. *Multiscale modelling of metallic nanoparticles structural and catalytic properties.* PhD Thesis, KCL (2018).

[69] H. Moerkved. *Exploring CO2 reduction on Cu from a geometrical perspective with the NanoCHE model.* MSc Thesis, KCL (2019).

[70] K.Rossi et al. *Screening and Designing Pt-nanoparticle isomers for Oxygen Reduction.* ACS Catal. 2020, 10, 6, 3911-3920.

[71] JK. Nørskov et al. *Origin of the Overpotential for Oxygen Reduction at a Fuel-Cell Cathode.* J. Phys. Chem. B 2004, 108, 17886–17892.

[72] M.Ichimura. *Atomic Structure of Surface Steps and Reconstruction.* Encyclopedia of Materials: Science and Technology, 2001, 383 - 387.

[73] J.Suzanne et al. *The Structure of Physically Adsorbed Phases.* Handbook of Surface Science, Vol. 1, 1996, 503-575.

[74] L. Gautier https://pypi.org/project/rpy2/, 2020, 3.

[75] E.L. Clarket al. *Standards and Protocols for Data Acquisition and Reporting for Studies of the Electrochemical Reduction of Carbon Dioxide.* ACS Catal. 2018, 8, 6560 -6570.

[76] S. Lewis et al. *Powering the Planet: Chemical Challenges in Solar Energy Utilization.* Proc. Natl. Acad. Sci. 2006, 103, 15729-15735.

[77] S. Chuet al. *Opportunities and Challenges for a Sustainable Energy Future.* Nature 2012, 488, 294-303.

[78] Z. Seh et al. *Combining Theory and Experiment in Electrocatalysis: Insights into Materials Design.* Science 2017, 355, 1-12.

[79] J.E. Pander et al. *Practices for the Collection and Reporting of Electrocatalytic Performance and Mechanistic Information for the CO_2 Reduction Reaction.* Catal. Sci. Technol. 2017, 7, 5820-5832.

[80] Kortlever et al. *Catalysts and reaction pathways for the electrochemical reduction of carbon dioxide.* J Phys Chem Lett 6:4073–4082.

[81] Y. Hori. *CO_2 reduction using electrochemical approach. Solar to Chemical Energy Conversion: Theory and Application.* Springer International, Cham, Switzerland, 191–211.

[82] F. Balettoet al. *Crossover among structural motifs in transition and noble-metal clusters.* J. Chem. Phys.2002, 116, 3856.